Research Square

Preprints are preliminary reports that have not undergone peer review.
They should not be considered conclusive, used to inform clinical practice,
or referenced by the media as validated information.

NXPH4 coordinates DNA repair and macrophage polarization to promote chemoresistance in colorectal cancer

Weijian Guo

guoweijian1@hotmail.com

Fudan University Shanghai Cancer Center, Shanghai, P.R. China https://orcid.org/0000-0002-6155-8345

jinsi Chen

Fudan University Shanghai Cancer Center

Tianyu Su

Fudan University Shanghai Cancer Center

Yanan Yang

Fudan University Shanghai Cancer Center

Kaiyue Yu

Jieyun Zhang

Department of Medical Oncology, Fudan University Shanghai Cancer Center, Shanghai, P.R. China

Shenglin Huang

Fudan University Shanghai Cancer Center & Institutes of Biomedical Sciences,Fudan University https://orcid.org/0000-0003-1279-0794

Article

Keywords: Colorectal cancer, Chemoresistance, NXPH4, hnRNPC, DNA damage repair, Macrophage polarization

Posted Date: September 1st, 2026

DOI: https://doi.org/10.21203/rs.3.rs-10604637/v1

License: This work is licensed under a Creative Commons Attribution 4.0 International License. Read Full License

Additional Declarations: (Not answered)

Abstract

Chemoresistance remains a major barrier to effective treatment of advanced colorectal cancer (CRC). Neurexophilin-4 (NXPH4), a secreted glycoprotein linked to tumor progression, has not been mechanistically defined in CRC chemoresistance. We integrated transcriptomic datasets from chemotherapy-sensitive and -resistant CRC tissues and evaluated NXPH4 expression in clinical samples and CRC models. In a plasma cohort of 190 patients with metastatic CRC, higher NXPH4 levels were associated with chemotherapy non-response and shorter overall and progression-free survival, with moderate discriminatory performance for treatment response (AUC = 0.773). Mechanistically, nuclear NXPH4 interacted with hnRNPC and was associated with increased hnRNPC protein stability, MCM2-7 expression, and resistance to chemotherapy-induced DNA damage. Secreted NXPH4 altered macrophage cholesterol homeostasis by suppressing ABCA1 and ABCG1 and was associated with a STAT6-PPARγ-linked M2-like phenotype. Conditioned medium from NXPH4-treated macrophages reduced CRC cell sensitivity to oxaliplatin and 5-fluorouracil. Upstream, ZNF263 promoted NXPH4 transcription through promoter binding. Collectively, these findings identify NXPH4 as a candidate biomarker and mechanistic contributor to CRC chemoresistance and suggest that NXPH4 links tumor-intrinsic DNA damage responses with macrophage immunometabolic remodeling.

Introduction

Colorectal cancer (CRC) remains a major cause of cancer morbidity and mortality worldwide [1]. In China, the burden is particularly severe, with approximately 578,000 new cases reported in 2024, and the incidence continues to rise among younger populations [2, 3]. Despite advances in targeted therapy and immunotherapy, platinum-based chemotherapy remains the first-line treatment for advanced CRC. The FOLFOX regimen (5-fluorouracil, leucovorin, and oxaliplatin) or XELOX regimen (capecitabine plus oxaliplatin) significantly improves patient survival; however, the development of chemoresistance leads to treatment failure in the majority of patients [4, 5]. Therefore, elucidating the molecular mechanisms underlying chemoresistance and identifying predictive biomarkers are critical for achieving precision therapy in CRC.

Chemoresistance is a complex biological process involving multiple mechanisms, including drug efflux, DNA damage repair (DDR) enhancement, apoptosis evasion, epithelial-mesenchymal transition, and metabolic reprogramming [6, 7]. Among these, enhanced DDR capacity is a major contributor to platinum-based chemoresistance. Oxaliplatin induces DNA crosslinks that block replication and transcription, while 5-fluorouracil inhibits thymidylate synthase and induces replication fork stalling [8, 9]. Efficient repair of these lesions enables tumor cell survival. The MCM2-7 helicase complex, a core component of the DNA replication machinery, plays a pivotal role in DDR by facilitating DNA replication restart and repair [10, 11]. RNA-binding proteins (RBPs), particularly heterogeneous nuclear ribonucleoproteins (hnRNPs), have emerged as key regulators of mRNA stability and translation, thereby influencing DDR and chemoresistance [12, 13].

Tumor-associated macrophages (TAMs) constitute the most abundant immune cell population in the tumor microenvironment (TME) and are predominantly polarized toward the M2 phenotype, which promotes tumor immune evasion, angiogenesis, and metastasis [14, 15]. Recent studies have highlighted the importance of cholesterol metabolism reprogramming in driving M2 polarization [16, 17]. Lipid-laden foamy macrophages exhibit typical M2 characteristics, with lipid droplets serving as signaling platforms that recruit various molecules to regulate inflammatory responses [18]. Cholesterol efflux transporters ABCA1 and ABCG1, together with cholesterol esterification enzyme ACAT1, coordinately regulate macrophage cholesterol homeostasis and polarized phenotype [16, 19]. However, the mechanisms by which tumor-secreted factors modulate macrophage cholesterol metabolism remain incompletely understood.

Neurexophilin-4 (NXPH4) is a member of the neurexophilin protein family, initially characterized as a regulator of synaptic function in the nervous system [20]. Recent studies have revealed its aberrant expression and oncogenic roles in various malignancies, including bladder cancer, prostate cancer, non-small cell lung cancer, and oral squamous cell carcinoma [21–23]. NXPH4 has been reported to promote tumor cell proliferation, migration, and resistance to enzalutamide in prostate cancer by modulating mitochondrial metabolism [24]. In colorectal cancer, NXPH4 was identified as a prognostic biomarker associated with metabolic reprogramming and immune infiltration [25]. However, the function of NXPH4 in CRC chemoresistance and its underlying molecular mechanisms remain largely unexplored.

In this study, we identified NXPH4 as a critical mediator of CRC chemoresistance through multi-dimensional differential gene analysis. We aimed to demonstrate that NXPH4 exhibits both intracellular and extracellular functions: nuclear-localized NXPH4 binds to hnRNPC, stabilizes MCM2-7 mRNA, and enhances DDR; while secreted NXPH4 reprograms macrophage cholesterol metabolism, driving M2 polarization via the STAT6-PPARγ axis. Furthermore, we identified ZNF263 as a transcriptional activator of NXPH4, establishing the ZNF263-NXPH4 regulatory axis. These findings provide a comprehensive understanding of NXPH4-mediated chemoresistance and identify potential therapeutic targets for overcoming drug resistance in CRC.

Materials and Methods

Clinical samples

CRC tissues, adjacent normal tissues, and plasma samples were collected from patients at Fudan University Shanghai Cancer Center (FUSCC) with informed consent and approval from the Ethics Committee of FUSCC (approval number: 050432-4-2108). A total of 190 plasma samples from metastatic CRC patients were collected prior to first-line chemotherapy. Tumor response was evaluated according to RECIST 1.1 criteria. Progression-free survival (PFS) was defined as the time from treatment initiation to disease progression or death. Overall survival (OS) was defined as the time from treatment initiation to death from any cause.

Cell lines and culture

Human CRC cell lines (HCT116, RKO, SW480, DLD1, HT29, SW620, HCT8), normal colonic epithelial cell line NCM460, human embryonic kidney cell line HEK-293T, and mouse CRC cell lines CT26 and MC38 were obtained from the American Type Culture Collection (ATCC). Oxaliplatin-resistant (RKO-OxaR) and 5-fluorouracil-resistant (RKO-5FUR) cell lines were established by continuous exposure to increasing concentrations of the respective drugs. Cells were cultured in DMEM or RPMI 1640 medium supplemented with 10% fetal bovine serum (FBS) and 1% penicillin-streptomycin at 37℃ in a humidified atmosphere with 5% CO2.

Plasmid construction, lentivirus packaging and cell transfection

Lentiviral overexpression vectors for NXPH4, hnRNPC, and ZNF263 were purchased from Diying Biotech, whereas the NXPH4 shRNA plasmid was obtained from Tsingke Biotechnology. The corresponding target sequences are provided in **Supplementary Table S1**. For viral production, HEK-293T cells were transfected with the respective overexpression or shRNA plasmids together with the packaging plasmid psPAX2 and the envelope plasmid pMD2.G (Addgene) using JetPRIME reagent. The viral supernatants were collected at 48 h post-transfection, and titers were subsequently determined. CRC cells were then transduced with recombinant lentivirus at 1×10^6 transducing units in the presence of 10 μg/ml polybrene (Beyotime).

RNA interference

Gene-specific siRNAs against NXPH4, hnRNPC, and ZNF263, along with negative control oligonucleotides, were chemically synthesized by Tsingke Biotech (China). Cells were transfected with the designated siRNAs or control duplexes using Lipofectamine RNAiMAX reagent (Invitrogen, USA) at a final concentration of 50 nM. At 48 h post-transfection, cells were harvested for downstream analyses including CCK-8 assay, RNA extraction, and Western blotting. The siRNA target sequences are detailed in **Supplemental Table S1**.

RNA extraction and quantitative real-time RT-PCR (RT-qPCR)

Total RNA was extracted from cells and tissues using the Total RNA Extraction Kit (NCM Biotech). Equal amounts of RNA were reverse transcribed into complementary DNA (cDNA) for qPCR template preparation with the reverse transcription premix kit (Accurate Biology, Cat. No. AG11706). RT-qPCR amplification was performed on an ABI Prism 7500 System (Applied Biosystems, Carlsbad, CA, USA) using the qPCR detection kit (Accurate Biology, Cat. No. AG11718). The relative gene expression levels were calculated by the $2^{-\Delta\Delta Ct}$ method, and the cycle threshold (Ct) values of target genes were normalized to the internal reference gene GAPDH. The primer sequences of NXPH4, MCM2-7, hnRNPC,

ZNF263, ABCA1, ABCG1, CD163, CD206, IL10, CD80, CD86 and iNOS are listed in **Supplemental Table S2.**

Western blot analysis

Total proteins were extracted from whole-cell lysates, resolved by SDS-PAGE, and transferred onto PVDF membranes (Millipore). The membranes were blocked and incubated with primary antibodies overnight at 4℃, followed by 1 h exposure to HRP-conjugated secondary antibodies at room temperature. Protein bands were visualized using an enhanced chemiluminescence reagent (ShareBio, China). β-Actin or GAPDH was used as a loading control. Antibody details are summarized in **Supplemental Table S3**.

Cell proliferation and colony formation assays

Cell proliferation was assessed using Cell Counting Kit-8 (CCK-8) reagent (YEASEN, China) in accordance with the supplier's protocol. For the colony formation assay, cells were seeded at low density into 6-well plates and maintained at 37℃ for 7–14 days. The formed colonies were fixed with 4% phosphate-buffered formalin (pH 7.4) and stained with crystal violet for 15 min.

Enzyme-linked Immunosorbent assay (ELISA)

Plasma and cell culture supernatants were collected in endotoxin-free tubes and analysed by ELISA according to the manufacturer's instructions (Shenrui biotech, Shanghai, China). Briefly, samples and serially diluted standards (50 μL) were added to the plate and incubated at 37℃ for 50 min. After washing three times, 100 μL of 1×biotinylated antibody working solution was added and incubated at 37℃ for 50 min. Following another wash, 100 μL of 1×SABC working solution was added and incubated at 37℃ for 30 min. The plate was washed again, and 100 μL of TMB substrate was added for color development at 37℃ in the dark for 10–20 min. The reaction was terminated by adding 50 μL of stop solution, and absorbance was measured at 450 nm within 30 min. Sample concentrations were determined by interpolation from the standard curve and multiplied by the dilution factor.

IC50 determination

Cells were plated and treated with serial concentrations of Oxa and 5-FU. After 48h, 100 μL of CCK-8 reagent was added per well and incubated for another 2 h. Cell throughbility was determined by measuring absorbance at 450 nm with a microplate reader. The IC50 of Oxa and 5-FU was calculated using GraphPad Prism 9.0.

Flow cytometry analysis

For cell cycle profiling, cells were rinsed twice with ice-cold PBS, fixed in 70% pre-cooled ethanol at 4℃ overnight, and then stained with a mixture containing 10 mg/ml RNase and 400 mg/ml propidium iodide

(PI) for 30 min at 37℃ in the dark before flow cytometric analysis.

For apoptosis detection, cells were collected, washed, and stained with PE-conjugated Annexin V and 7-AAD for 15 min at room temperature in the dark. Flow cytometric analysis was performed within 1 h. All experiments were independently repeated three times with triplicate samples per assay.

Mouse tumor tissues were cut into small fragments and enzymatically digested with 1 mg/mL collagenase V and 4 μg/mL DNase I (Worthington) at 37℃ for 1 h. Erythrocytes were subsequently depleted using RBC lysis buffer (BioLegend), and the resulting cell suspensions were filtered through a 70-μm cell strainer to obtain single-cell preparations. Macrophage populations were identified by staining with BV605-CD45, PerCP/Cyanine5.5-CD11b, and PE-F4/80. M1 macrophages were further distinguished using APC-CD86, whereas M2 tumor-associated macrophages were detected with PE/Cyanine7-CD206. Following three washes, cells were resuspended and analysed by flow cytometric analysis. In human THP-1-derived macrophages, M1 polarization was evaluated using APC-CD86, and M2 polarization was assessed using FITC-CD206. Antibody details are also summarized in **Supplemental Table S3**.

Immunoprecipitation and mass spectrometry

Cells were lysed in IP lysis buffer containing protease and phosphatase inhibitors. Lysates were incubated with anti-FLAG magnetic beads (Tianjin Nuoyi Biotech, China, Cat. No. FNM-25-500) overnight at 4℃. After washing, bound proteins were eluted and separated by SDS-PAGE. Gel bands were excised, digested with trypsin, and analyzed by liquid chromatography-tandem mass spectrometry (LC-MS/MS) using an Easy-nLC 1200 system coupled to a Q Exactive Plus mass spectrometer.

Co-immunoprecipitation

Cells were lysed in IP lysis buffer and incubated with primary antibodies overnight at 4℃, followed by incubation with Protein A/G magnetic beads (MedChemExpress). For Western blotting, proteins were separated by SDS-PAGE, transferred to PVDF membranes, and probed with specific primary antibodies. Signals were detected using enhanced chemiluminescence reagents.

Immunofluorescence confocal imaging

Cells were fixed with 4% paraformaldehyde at room temperature, permeabilized in 0.1% Triton X-100/PBS for 30 min, and subsequently incubated with primary antibody overnight, followed by secondary antibodies (1h, room temperature) and DAPI. Antibody information is provided in **Supplemental Table S3**. The DNA Damage Assay Kit based on γ-H2AX immunofluorescence (Beyotime, China, Cat. No. C2037S) was used to evaluate γ-H2AX expression.

Luciferase assay

The NXPH4 promoter region (-2000bp to + 100 bp) was cloned into the pGL4.10 vector. Cells were co-transfected with reporter plasmids and Renilla luciferase plasmids. Luciferase activity was measured

using the Dual-Luciferase Reporter Assay System (Promega, Cat. No. E1910) and normalized to Renilla activity.

Chromatin immunoprecipitation quantitative PCR (ChIP-qPCR)

ChIP assays were performed according to the manufacturer's instructions of the ChIP kit (CST, Cat. No. #9003). Cells were cross-linked with 1% formaldehyde, lysed, and sonicated to generate DNA fragments of 150–900 bp. Chromatin was immunoprecipitated with anti-FLAG magnetic beads. After reverse cross-linking and DNA purification, qPCR was performed using specific primers targeting predicted ZNF263 binding sites.

Animal studies

All animal experiments were approved by the Ethics Committee of Fudan University Shanghai Cancer Center (approval number: FUSCC-IACUC-2025498, FUSCC-IACUC-2024618) and conducted in accordance with the institutional guidelines for animal care and use.

BALB/c nude mice (6 weeks old) were subcutaneously injected with 5×10^6 DLD1 cells stably expressing shNC or shNXPH4. When tumors reached approximately 5 mm in diameter, mice were randomized and treated with oxaliplatin (5 mg/kg) or vehicle (5% glucose) intraperitoneally every 3 days. Tumor volume was calculated as (length×width^2)/2.

Six- to eight-week-old C57BL/6 mice were subcutaneously injected with 5×10^5 MC38 cells (control [PCDH], stable NXPH4-overexpressing, control [sgScramble], or sgNxph4). Upon tumor establishment, tumor dimensions and body weight were monitored every 2–3 days. Tumor volume was calculated as (length × width^2) / 2.

Immunohistochemistry (IHC)

Tumor tissues were fixed in 4% paraformaldehyde for 24 h, paraffin-embedded, and sectioned at 4 μm. After dewaxing and rehydration, antigen retrieval was performed in 10 mM sodium citrate buffer (pH 6.0) by microwave heating for 20 min. Endogenous peroxidase was blocked with 3% H_2O_2 for 25 min, followed by 3% BSA blocking for 30 min. Sections were incubated with primary antibody overnight at 4°C and then with HRP-conjugated secondary antibody for 50 min at room temperature. Signals were developed with DAB and counterstained with hematoxylin. Antibody information is provided in **Supplemental Table S3**.

Statistical analysis

Data are presented as mean ± standard dethroughtion (SD) from at least three independent experiments. Statistical analysis was performed using GraphPad Prism 9.0 (GraphPad Software, San Diego, CA, USA). Differential gene expression analysis from RNA sequencing data was conducted using the R package "DESeq2" (version 1.38.0). Statistical significance was determined using Student's t-test for two-group

comparisons or one-way ANOVA with Bonferroni correction for multiple comparisons. Survival analysis was performed using the Kaplan-Meier method with log-rank test. Correlation analysis was performed using Spearman's rank correlation. A p-value < 0.05 was considered statistically significant.

Results

NXPH4 is identified as a candidate secreted protein associated with CRC chemoresistance and poor prognosis

To identify secreted molecules associated with CRC chemoresistance, we integrated RNA sequencing datasets from chemotherapy-sensitive and -resistant tissues, and paired tumor and adjacent normal tissues. Differentially expressed genes were intersected with secreted proteins annotated in the Human Protein Atlas database. Fourteen molecules were identified as significantly upregulated in both chemoresistant tissues and colorectal cancer tissues. Among these 14 candidates, five molecules (IGF2, VGF, TNFRSF11B, TFF2, and PRSS2) have been implicated in therapy resistance or tumor progression in various malignancies [26–32]. The remaining nine candidates (LBP, LPO, FREM1, CEL, F7, ISM2, FGB, and CSTL1) lack established reports linking them to chemoresistance, representing potentially novel mediators of drug resistance. NXPH4 was identified as a significantly upregulated secreted protein in chemoresistant samples and was selected for further investigation **(**Fig. 1A**)**. Analysis of GEO (GSE87211) and TCGA datasets, together with cell-line validation, confirmed higher NXPH4 expression in CRC tissues and cell lines than in normal counterparts **(Supplemental Figure S1A-C)**. High NXPH4 expression was also associated with shorter overall survival in both cohorts **(Supplemental Figure S1D-E)**. We next measured plasma NXPH4 in 190 metastatic CRC patients before first-line chemotherapy. Plasma NXPH4 levels were higher in non-responders than in responders (Fig. 1B), and ROC analysis showed moderate predictive performance for chemotherapy non-response (AUC = 0.773, 95% CI: 0.710–0.836, p < 0.001) (Fig. 1C). Patients with high plasma NXPH4 had shorter overall and progression-free survival than those with low plasma NXPH4 **(**Fig. 1D-E**)**. Baseline clinicopathological characteristics were comparable between the two groups **(Supplemental Table S4)**. Furthermore, analysis of single-cell transcriptome data from the GSE132465 dataset showed predominant expression of NXPH4 within tumour epithelial cells, indicating tumour epithelial cells are the main source of NXPH4 in CRC tissues **(**Fig. 1J**-K)**. These data nominate NXPH4 as a candidate biomarker for chemotherapy response and outcome, although independent validation is required.

NXPH4 promotes CRC cell proliferation and chemoresistance in CRC cells

To investigate the role of NXPH4 in CRC, we established stable NXPH4-overexpressing and knockdown cell lines **(Supplemental Figure S2A)**. CCK-8 and colony formation assays showed that NXPH4 overexpression promoted cell proliferation, while knockdown inhibited proliferation **(Supplemental**

Figure S2C-F). Recombinant NXPH4 protein treatment also promoted CRC cell proliferation **(Supplemental Figure S2G)**, indicating that secreted NXPH4 is biologically active.

To assess the effect of NXPH4 on chemoresistance, we performed IC50 assays. NXPH4 overexpression significantly increased the IC50 values of oxaliplatin and 5-fluorouracil in RKO and HCT116 cells **(**Fig. 2A**)**. Conversely, NXPH4 knockdown decreased the IC50 values in SW480 and HCT116 cells **(**Fig. 2B**)**. Colony formation assays confirmed that NXPH4 overexpression conferred resistance to oxaliplatin and 5-fluorouracil, while knockdown sensitized cells to these drugs **(**Fig. 2C**)**. Furthermore, knockdown of NXPH4 in resistant cell lines significantly inhibited their proliferation **(**Fig. 2D**)**. Apoptosis assays demonstrated that NXPH4 knockdown promoted oxaliplatin- and 5-fluorouracil-induced apoptosis **(**Fig. 2E**)**. Subsequently, RKO colorectal cancer cells were exposed to oxaliplatin (Oxa) for 48 h, and Western blot analysis was performed to assess the expression of apoptosis-related proteins BCL2, BAX, and Caspase-3. The results demonstrated that BAX and cleaved caspase-3 levels were significantly elevated in the shNXPH4 group upon oxaliplatin treatment, whereas expression of the anti-apoptotic molecule BCL2 was markedly decreased **(**Fig. 2F**)**. These results establish NXPH4 as a critical regulator of CRC chemoresistance.

NXPH4 promotes chemoresistance through DNA damage repair in vitro and in vivo

To investigate the mechanism by which NXPH4 promotes chemoresistance, we performed RNA sequencing on NXPH4-overexpressing cells. KEGG pathway enrichment analysis revealed significant upregulation of cell cycle, DNA replication, and DNA repair pathways **(**Fig. 3A**)**. Notably, A significant enrichment of genes associated with DNA repair and cell cycle regulation was identified, exemplified by the MCM family genes **(**Fig. 3B**)**. These findings were then functionally tested in CRC cells. Overexpression of NXPH4 promoted cell cycle progression **(**Fig. 3C**)**, whereas its knockdown had the opposite effect **(**Fig. 3D**)**. Immunofluorescence detection of the DNA damage marker γ-H2AX revealed that NXPH4 knockdown increased both γ-H2AX expression and the number of positive cells, while NXPH4 overexpression reduced γ-H2AX levels **(**Fig. 3E**)**. Moreover, under Oxa treatment, NXPH4 overexpression significantly suppressed Oxa-induced γ-H2AX expression **(**Fig. 3F**)**. Together, these results support the conclusion that NXPH4 drives proliferation and chemoresistance in CRC cells by accelerating cell cycle progression and supporting DNA damage repair.

To test whether NXPH4 influences the chemotherapeutic response of CRC in vivo, DLD1 cells with stable NXPH4 knockdown were generated and subcutaneously inoculated into nude mice. When tumour diameters reached approximately 5 mm, mice were intraperitoneally treated with either 5 mg/mL oxaliplatin (Oxa) or an equal volume of 5% glucose solution (5% GS), for a total of six drug administrations **(**Fig. 3G**)**. Compared with the shNC + 5% GS control group, NXPH4 knockdown (shNXPH4 + 5% GS) significantly suppressed tumour proliferation in vivo. Under oxaliplatin treatment, the shNXPH4 group exhibited a smaller increase in tumour volume compared with the shNC group **(**Fig. 3H**-I)**. Consistently, tumour weight was also lower in the shNXPH4 group than in the control shNC

group (Fig. 3J). Following oxaliplatin treatment, the shNXPH4 + Oxa group also showed reduced tumour volume (Fig. 3H-**I**) and lower tumour weight (Fig. 3J) relative to the control shNC + Oxa group. No significant effect of the drug dose on body weight was observed in the shNXPH4 group. After day 18, body weight declined in both shNC-containing groups, likely due to the increased tumour burden (Fig. 3K).

Immunohistochemical analysis was then performed on the subcutaneous tumour tissues from the Oxa-treated groups to evaluate the expression of Ki67, cleaved caspase-3, and γ-H2AX. Compared with the 5% GS-treated group, Oxa-treated tumours showed significantly reduced Ki67 expression and markedly increased levels of cleaved caspase-3 and γ-H2AX. Furthermore, within the Oxa-treated groups, the shNXPH4 group exhibited lower Ki67 expression and higher levels of cleaved caspase-3 and γ-H2AX compared with the shNC group (Fig. 3L). Together, these findings indicate that NXPH4 regulates chemoresistance in CRC through DNA damage repair mechanisms.

Nuclear-localized NXPH4 promotes DNA damage repair through the hnRNPC-MCM2-7 axis

Although NXPH4 contains a classical signal peptide, immunofluorescence staining of colorectal cancer tissues also revealed nuclear localization (Fig. 4A). NLS prediction identified a species-conserved nuclear localization signal in NXPH4 (Fig. 4B), and nuclear fractionation confirmed detectable NXPH4 in the nuclear fraction of NXPH4-overexpressing CRC cells (**Supplemental Figure S3A**). To define the function of this nuclear pool, we performed immunoprecipitation-mass spectrometry and identified hnRNPC as a candidate NXPH4-interacting protein (Fig. 4C). Subcellular fractionation showed that both NXPH4 and hnRNPC were present in the nuclear fraction (**Supplemental Figure S4B**). Co-immunoprecipitation confirmed the NXPH4-hnRNPC interaction (Fig. 4D), and immunofluorescence showed nuclear colocalization of NXPH4 and hnRNPC (Fig. 4E).

To map the binding domain, we constructed hnRNPC truncation mutants. Co-immunoprecipitation experiments demonstrated that NXPH4 bound to the bZLM domain (amino acids 140–214) of hnRNPC (Fig. 4F-G). NXPH4 knockdown decreased hnRNPC protein levels without affecting its mRNA levels, suggesting post-transcriptional regulation (Fig. 4H-I). Treatment with the proteasome inhibitor MG-132 rescued the decrease in hnRNPC protein levels upon NXPH4 knockdown (Fig. 4J). Cycloheximide chase assays showed that NXPH4 knockdown shortened the half-life of hnRNPC protein (Fig. 4K). Furthermore, ubiquitination assays demonstrated that NXPH4 knockdown increased hnRNPC ubiquitination (Fig. 4L). These results indicate that NXPH4 binds to hnRNPC and inhibits its ubiquitin-proteasome degradation.

Bulk RNA sequencing showed upregulation of MCM2-7 complex genes upon NXPH4 overexpression (**Supplemental Figure S3C**), which was conversely validated by RT-qPCR demonstrating marked downregulation of these genes following NXPH4 knockdown (**Supplemental Figure S3D**). Correlation analysis using TCGA data showed positive correlations between NXPH4 and MCM2-7 expression (**Supplemental Figure S3E**). Western blotting confirmed that NXPH4 knockdown decreased MCM2-7

protein levels **(Supplemental Figure S3F)**. To investigate the mechanism by which NXPH4 regulates MCM2-7 expression, we focused on hnRNPC, a canonical RNA-binding protein that governs mRNA splicing, stability, nucleocytoplasmic transport, and translation [12, 13]. Previous studies have demonstrated that hnRNPC stabilizes MCM3 mRNA to enhance its expression [33], suggesting a potential regulatory role of hnRNPC in controlling MCM2-7 expression.

To determine whether hnRNPC mediates the effect of NXPH4 on MCM2-7, we performed rescue experiments. hnRNPC overexpression reversed the decrease in cell proliferation **(Supplemental Figure S3G-H)** and the increase in chemosensitivity caused by NXPH4 knockdown **(Supplemental Figure S3I-J)**. RNA stability assays demonstrated that hnRNPC overexpression extended the half-life of MCM2-7 mRNA **(Supplemental Figure S3K)**. hnRNPC overexpression also rescued the decrease in MCM2-7 mRNA and protein levels caused by NXPH4 knockdown **(Supplemental Figure S3F, S3L)**. These findings establish the NXPH4-hnRNPC-MCM2-7 axis as a critical pathway for DNA damage repair and chemoresistance.

Secreted NXPH4 induces M2 macrophage polarization through cholesterol metabolism reprogramming

To investigate the role of secreted NXPH4 in the tumor microenvironment, we established MC38 mouse models with Nxph4 overexpression or knockout. Nxph4 overexpression significantly promoted tumor growth **(**Fig. 5A-C**)**, while knockout inhibited growth **(Supplemental Figure S4A-C)**. RNA sequencing and immune infiltration analysis revealed increased M2 macrophage infiltration in Nxph4-overexpressing tumors **(**Fig. 5D**)**. Flow cytometry confirmed increased CD206 + M2 macrophages in Nxph4-overexpressing tumors **(**Fig. 5E**)** and decreased M2 macrophages in Nxph4-knockout tumors **(Supplemental Figure S4D)**. Immunohistochemistry showed elevated Ki67 and CD163 expression in Nxph4-overexpressing tumors **(**Fig. 5F**)**. However, Nxph4 knockout significantly reduced Ki67 and CD206 expression of tumor tissues **(Supplemental Figure S4E)**.

To test directly the effect of NXPH4 on macrophage polarization, we treated THP-1-derived macrophages with recombinant NXPH4 protein. Flow cytometry demonstrated that NXPH4 treatment increased the proportion of CD206 + M2 macrophages in a dose-dependent manner without affecting CD86 + M1 macrophages **(**Fig. 5G-H**)**. Western blotting and RT-qPCR confirmed upregulation of M2 markers (CD163, IL10, CD206) without changes in M1 markers (CD86, CD80, iNOS) **(**Fig. 5I**)**. Transwell migration assays showed that NXPH4 promoted macrophage migration **(Supplemental Figure S4F)**. Conditioned medium from NXPH4-treated macrophages decreased the chemosensitivity of CRC cells to oxaliplatin and 5-fluorouracil **(**Fig. 5J-K**)**.

To investigate the mechanism of NXPH4-induced M2 polarization, we performed RNA sequencing on NXPH4-treated macrophages. KEGG pathway analysis revealed significant enrichment of cholesterol metabolism pathways **(**Fig. 5L**)**. Cholesterol efflux genes ABCA1 and ABCG1 were significantly downregulated **(Supplemental Figure S4G)**. RT-qPCR validated the dose-dependent downregulation of

ABCA1 and ABCG1 by NXPH4 (Fig. 5M). Lipid droplet staining demonstrated increased lipid accumulation in NXPH4-treated macrophages (Fig. 5N). Western blotting showed activation of the STAT6-PPARγ axis, with increased phosphorylated STAT6 and PPARγ expression (Fig. 5O). ACAT1, a key enzyme in cholesterol esterification, was also upregulated (Fig. 5O). Biochemical assays confirmed increased total cholesterol and cholesterol esters with decreased free cholesterol in NXPH4-treated macrophages (Fig. 5P-R). These results indicate that NXPH4 reprograms macrophage cholesterol metabolism by downregulating ABCA1/ABCG1, leading to lipid accumulation and STAT6-PPARγ-mediated M2 polarization.

ZNF263 activates NXPH4 transcription to promote chemoresistance

To identify the upstream transcriptional regulator of NXPH4, we performed bioinformatics analysis using UCSC, ChIP-Atlas, GTRD, and hTFtarget databases. ZNF263 emerged as a candidate transcription factor (Fig. 6A). Correlation analysis using FUSCC and GSE87211 datasets revealed a significant positive correlation between ZNF263 and NXPH4 expression (Fig. 6B). ZNF263 knockdown decreased NXPH4 mRNA and protein levels, while ZNF263 overexpression increased NXPH4 expression (Fig. 6D-E). Dual-luciferase reporter assays demonstrated that ZNF263 overexpression significantly activated the NXPH4 promoter (Fig. 6F). JASPAR database prediction identified three potential ZNF263 binding sites in the NXPH4 promoter (Fig. 6G). ChIP-qPCR confirmed that ZNF263 bound to all three sites (Fig. 6H-I), establishing ZNF263 as a direct transcriptional activator of NXPH4. TCGA colorectal cancer cohort data revealed that ZNF263 expression levels were significantly positively correlated with the IC50 values of Oxa and 5-FU, suggesting that ZNF263 serves as a critical driver of Oxa and 5-FU resistance in colorectal cancer (Fig. 6K-L). ZNF263 overexpression increased the IC50 values of Oxa and 5-FU (Fig. 6M-N). Importantly, knockdown of NXPH4 reversed the chemoresistance induced by ZNF263 overexpression (Fig. 6M-N). These results demonstrate that the ZNF263-NXPH4 axis promotes CRC chemoresistance.

Discussion

This study identifies NXPH4 as a coordinator of tumor-intrinsic and microenvironmental mechanisms of CRC chemoresistance. Our data support a model in which ZNF263-induced NXPH4 promotes hnRNPC-dependent MCM2-7 expression and DNA damage repair-associated resistance in tumor cells, while secreted NXPH4 promotes macrophage immunometabolic remodeling through an ABCA1/ABCG1- and STAT6-PPARγ-associated program (Fig. 7).

We identified NXPH4 as a critical mediator of CRC chemoresistance through multi-dimensional differential gene analysis integrating chemotherapy-sensitive and -resistant tissues, pre- and post-chemotherapy tissues, as well as tumor and adjacent normal tissues. NXPH4 was significantly upregulated in CRC tissues, chemoresistant patient samples, and drug-resistant cell lines. Notably, NXPH4 secretion was markedly enhanced in oxaliplatin-resistant and 5-fluorouracil-resistant cells, suggesting that chemotherapy stress may actively promote NXPH4 expression and secretion. This is

consistent with previous reports that chemotherapeutic agents such as cisplatin, paclitaxel, and doxorubicin can induce specific protein secretion through endoplasmic reticulum stress, autophagy-lysosomal pathways, or transcription factor activation [34, 35].

Plasma NXPH4 showed moderate predictive performance for chemotherapy response (AUC = 0.773) and was associated with shorter overall and progression-free survival in 190 metastatic CRC patients. These findings support plasma NXPH4 as a candidate liquid biopsy marker for patient stratification and treatment monitoring. However, its clinical utility remains to be established in prospective, multi-center cohorts and through comparison with conventional markers such as CEA and CA19-9.

Mechanistically, we found that NXPH4 exhibits nuclear localization in addition to its known secretory function. Through NLS prediction and subcellular fractionation, we confirmed that NXPH4 contains a species-conserved nuclear localization signal (amino acids 90–106) and is present in both cytoplasmic and nuclear compartments. This dual localization pattern is not unprecedented among secreted proteins; for example, IL-33 functions as a nuclear cytokine that regulates chromatin structure and gene transcription while also being released extracellularly to modulate immune responses [36]. Similarly, HMGB1 and β-catenin exhibit nucleocytoplasmic shuttling, with their subcellular localization determining distinct functional outcomes [37, 38].

Nuclear-localized NXPH4 binds to the bZLM domain (amino acids 140–214) of hnRNPC, inhibiting its ubiquitin-proteasome degradation. This interaction stabilizes hnRNPC protein, which in turn binds to and stabilizes MCM2-7 mRNA, enhancing DNA damage repair capacity. The MCM2-7 helicase complex is essential for DNA replication and repair, and its upregulation enables tumor cells to efficiently repair chemotherapy-induced DNA damage [10, 11]. Our findings reveal a novel post-transcriptional regulatory mechanism for MCM2-7 expression and identify NXPH4 as an upstream regulator of hnRNPC stability. This expands the known functions of hnRNPC in chemoresistance, which previously included stabilization of Nrf2 and SLC7A11 mRNA to inhibit ferroptosis in CRC [39], and m6A-dependent stabilization of TRAF6 and ALDH1A3 in pancreatic cancer [40].

The specificity of NXPH4-hnRNPC interaction is noteworthy. By constructing hnRNPC truncation mutants, we demonstrated that deletion of the bZLM domain completely abolished NXPH4 binding. The bZLM domain is critical for hnRNPC's RNA-binding activity and protein-protein interactions [41]. NXPH4 may protect hnRNPC from ubiquitination by masking specific lysine residues within or adjacent to the bZLM domain, or by sterically hindering E3 ubiquitin ligase access. Future studies employing mass spectrometry to identify hnRNPC ubiquitination sites and structural biology approaches to characterize the NXPH4-hnRNPC complex will be essential to elucidate the precise molecular mechanism.

Beyond its intracellular function, secreted NXPH4 plays a critical role in remodeling the tumor immune microenvironment. We demonstrated that NXPH4 induces M2 macrophage polarization through cholesterol metabolism reprogramming. NXPH4 downregulates the cholesterol efflux genes ABCA1 and ABCG1, leading to intracellular cholesterol accumulation, increased cholesterol esterification, and lipid droplet formation. This metabolic shift activates the STAT6-PPARγ axis, driving M2 polarization. Lipid-

laden "foamy" macrophages exhibit typical M2 characteristics and promote tumor immune evasion [16, 18]. Our findings establish a novel mechanism by which tumor-secreted factors modulate macrophage metabolism and function, distinct from previously reported mechanisms such as CAF-secreted GRP78 promoting M2 polarization through ATGL-mediated lipolysis [42], or tumor-derived IL-34 inducing CD36-mediated fatty acid uptake [17].

The activation of STAT6-PPARγ axis by cholesterol accumulation provides a mechanistic link. While IL-4/IL-13 are classical activators of STAT6 signaling [38], our data suggest that metabolic changes—specifically cholesterol esterification and lipid droplet accumulation—can independently activate this pathway. PPARγ serves as a metabolic sensor that translates transient STAT6 signals into sustained transcriptional programs by recruiting histone acetyltransferases and chromatin remodeling complexes [43]. The cholesterol metabolites or lipid droplet-derived signaling molecules may act as endogenous PPARγ ligands, although the identity of these ligands requires further investigation. Additionally, the CCL22 and CCL17 chemokines upregulated in NXPH4-overexpressing tumors may further amplify immunosuppression by recruiting regulatory T cells through CCR4 [44, 45].

We further identified ZNF263 as a direct transcriptional activator of NXPH4. ZNF263 belongs to the KRAB zinc finger protein family and has been linked to tumor progression and therapy resistance across multiple malignancies [46–50]. Our study extends current understanding of ZNF263 function in CRC by demonstrating its direct binding to three specific sites in the NXPH4 promoter (Site 1: -1406 to -1251; Site 2: -1181 to -1053; Site 3: -262 to -118) and activation of NXPH4 transcription. The ZNF263-NXPH4 axis promotes chemoresistance, as demonstrated by rescue experiments showing that NXPH4 knockdown reverses ZNF263-induced drug resistance.

The dual activity of NXPH4—both intracellular and extracellular—enables it to promote chemoresistance through multiple mechanisms simultaneously. Nuclear NXPH4 enhances DNA repair capacity in tumor cells, while secreted NXPH4 establishes an immunosuppressive microenvironment that further protects tumors from chemotherapy-induced immune responses. This multi-dimensional action makes NXPH4 an attractive therapeutic target, as its inhibition could both impair tumor cell DNA repair capacity and restore anti-tumor immune responses. Targeting the ZNF263-NXPH4-hnRNPC axis may represent a novel chemosensitization strategy, potentially through development of small molecule inhibitors or interfering peptides that disrupt specific protein-protein interactions.

Several limitations should be acknowledged. First, the specific receptor for NXPH4 on macrophages remains to be identified. While NXPH family proteins classically interact with neurexins [20], macrophages do not express neurexin-1, suggesting the existence of alternative receptors or internalization mechanisms. Second, the E3 ubiquitin ligase responsible for hnRNPC degradation and the specific ubiquitination sites require further investigation. Third, plasma NXPH4 as a biomarker needs validation in prospective, multi-center clinical trials with larger cohorts and comparison with established markers. Fourth, the in vivo experiments used subcutaneous xenograft models, which may not fully recapitulate the complexity of the human tumor microenvironment; orthotopic or patient-derived

xenograft models would provide more clinically relevant insights. Therefore, further investigation is necessary to gain a more precise understanding.

Conclusions

In conclusion, this study reveals the multi-dimensional roles of NXPH4 in promoting CRC chemoresistance. Our findings demonstrate that: (1) NXPH4 is upregulated in CRC and associated with chemoresistance and poor prognosis; (2) plasma NXPH4 is a promising biomarker for predicting chemotherapy response; (3) nuclear-localized NXPH4 binds to hnRNPC, stabilizes MCM2-7 mRNA, and enhances DNA damage repair; (4) secreted NXPH4 reprograms macrophage cholesterol metabolism, driving M2 polarization through the STAT6-PPARγ axis; and (5) ZNF263 activates NXPH4 transcription, forming a regulatory axis that promotes chemoresistance. These findings provide a broader understanding of NXPH4-mediated chemoresistance and identify the ZNF263-NXPH4-hnRNPC axis as a potential therapeutic target for overcoming drug resistance in CRC.

Abbreviations

ABCA1
ATP-binding cassette subfamily A member 1
ABCG1
ATP-binding cassette subfamily G member 1
ACAT1
Acyl-CoA:cholesterol acyltransferase 1
AUC
Area under the curve
ChIP-qPCR
Chromatin immunoprecipitation quantitative PCR
Co-IP
Co-immunoprecipitation
CRC
Colorectal cancer
DDR
DNA damage repair
hnRNPC
Heterogeneous nuclear ribonucleoprotein C
IP-MS
Immunoprecipitation-mass spectrometry
MCM
Minichromosome maintenance
NXPH4
Neurexophilin-4

OS
Overall survival
PFS
Progression-free survival
PPARγ
Peroxisome proliferator-activated receptor gamma
RBPs
RNA-binding proteins
ROC
Receiver operating characteristic
STAT6
Signal transducer and activator of transcription 6
TAMs
Tumor-associated macrophages
TME
Tumor microenvironment
ZNF263
Zinc finger protein 263

Declarations

Ethics approval

The collection of clinical data, tissue specimens and plasma samples was explained to all patients, and written informed consent was obtained from all participants. Tissue specimens and plasma samples used in this study were approved by the Ethics Committee of the FUSCC (approval number: 050432-4-2108). All animal experiments were approved by the Ethics Committee of Fudan University Shanghai Cancer Center (approval number: FUSCC-IACUC-2025498, FUSCC-IACUC-2024618) and conducted in accordance with the institutional guidelines for animal care and use.

Consent for publication

Not applicable.

Competing interests

The authors declare that they have no competing interests.

Funding

No funding

Authors’ contributions

Chen Jinsi conceptualized the study, designed the experiments, performed the majority of the in vitro and in vivo experiments, analyzed and interpreted the data, drafted the original manuscript, prepared the figures, and managed the submission and revision process. Su Tianyu assisted with the execution of selected experiments and contributed to the revision experiments during the peer-review process. Yang Ya’nan was responsible for the collection and processing of plasma specimens from metastatic colorectal cancer patients. Yu Kaiyue assisted with the execution of selected in vitro and in vivo experiments. Zhang Jieyun was responsible for the collection of clinical tissue specimens and contributed to the clinicopathological data analysis. Huang Shenglin and Guo Weijian supervised the entire project, secured resources, provided funding support, and critically revised the manuscript for important intellectual content. All authors read and approved the final manuscript.

Acknowledgements

We thank the Core Facilities of Fudan University Shanghai Cancer Center for technical assistance with flow cytometry, mass spectrometry, and immunohistochemistry. We are grateful to the staff of the Department of Gastrointestinal Medical Oncology at Fudan University Shanghai Cancer Center for their support in clinical sample collection and patient data management. We also thank the patients who participated in this study for their generous contribution of clinical samples and biological specimens.

Data availability

The datasets generated and/or analyzed during the current study are available from the corresponding author upon reasonable request.

References

1. Bray F, Laversanne M, Sung H, Ferlay J, Siegel RL, Soerjomataram I, et al. Global cancer statistics 2022: GLOBOCAN estimates of incidence and mortality worldwide for 36 cancers in 185 countries. CA Cancer J Clin. 2024;74:229–63. https://doi.org/10.3322/caac.21834.
2. Han B, Zheng R, Zeng H, Wang S, Sun K, Chen R, et al. Cancer incidence and mortality in China, 2022. Journal of the National Cancer Center. 2024;4:47–53. https://doi.org/10.1016/j.jncc.2024.01.006.
3. Eng C, Yoshino T, Ruíz-García E, Mostafa N, Cann CG, O’Brian B, et al. Colorectal cancer. The Lancet. Elsevier; 2024;404:294–310. https://doi.org/10.1016/S0140-6736(24)00360-X.
4. de Gramont A, Figer A, Seymour M, Homerin M, Hmissi A, Cassidy J, et al. Leucovorin and fluorouracil with or without oxaliplatin as first-line treatment in advanced colorectal cancer. J Clin Oncol. 2023;41:5080–9. https://doi.org/10.1200/JCO.22.02773.

5. Cassidy J, Clarke S, Díaz-Rubio E, Scheithauer W, Figer A, Wong R, et al. XELOX vs FOLFOX-4 as first-line therapy for metastatic colorectal cancer: NO16966 updated results. Br J Cancer. 2011;105:58–64. https://doi.org/10.1038/bjc.2011.201.
6. Holohan C, Van Schaeybroeck S, Longley DB, Johnston PG. Cancer drug resistance: An evolving paradigm. Nat Rev Cancer. 2013;13:714–26. https://doi.org/10.1038/nrc3599.
7. Vasan N, Baselga J, Hyman DM. A view on drug resistance in cancer. Nature. 2019;575:299–309. https://doi.org/10.1038/s41586-019-1730-1.
8. Longley DB, Harkin DP, Johnston PG. 5-fluorouracil: Mechanisms of action and clinical strategies. Nat Rev Cancer. 2003;3:330–8. https://doi.org/10.1038/nrc1074.
9. Martinez-Balibrea E, Martínez-Cardús A, Ginés A, Ruiz de Porras V, Moutinho C, Layos L, et al. Tumor-related molecular mechanisms of oxaliplatin resistance. Mol Cancer Ther. 2015;14:1767–76. https://doi.org/10.1158/1535-7163.MCT-14-0636.
10. Bochman ML, Schwacha A. The mcm complex: Unwinding the mechanism of a replicative helicase. Microbiol Mol Biol Rev. 2009;73:652–83. https://doi.org/10.1128/MMBR.00019-09.
11. Simon NE, Schwacha A. The Mcm2-7 replicative helicase: A promising chemotherapeutic target. Biomed Res Int. 2014;2014:549719. https://doi.org/10.1155/2014/549719.
12. Gerstberger S, Hafner M, Tuschl T. A census of human RNA-binding proteins. Nat Rev Genet. 2014;15:829–45. https://doi.org/10.1038/nrg3813.
13. Vembuli H, Gor R, Ramalingam S, Perales S, Rajasingh J. RNA binding proteins in cancer chemotherapeutic drug resistance. Front Cell Dev Biol. 2024;12:1308102. https://doi.org/10.3389/fcell.2024.1308102.
14. Cassetta L, Pollard JW. Targeting macrophages: Therapeutic approaches in cancer. Nat Rev Drug Discov. 2018;17:887–904. https://doi.org/10.1038/nrd.2018.169.
15. Mantovani A, Marchesi F, Malesci A, Laghi L, Allavena P. Tumour-associated macrophages as treatment targets in oncology. Nat Rev Clin Oncol. 2017;14:399–416. https://doi.org/10.1038/nrclinonc.2016.217.
16. Wu H, Han Y, Rodriguez Sillke Y, Deng H, Siddiqui S, Treese C, et al. Lipid droplet-dependent fatty acid metabolism controls the immune suppressive phenotype of tumor-associated macrophages. EMBO Mol Med. 2019;11:e10698. https://doi.org/10.15252/emmm.201910698.
17. Nian Z, Dou Y, Shen Y, Liu J, Du X, Jiang Y, et al. Interleukin-34-orchestrated tumor-associated macrophage reprogramming is required for tumor immune escape driven by p53 inactivation. Immunity. 2024;57:2344–2361.e7. https://doi.org/10.1016/j.immuni.2024.08.015.
18. Goossens P, Rodriguez-Vita J, Etzerodt A, Masse M, Rastoin O, Gouirand V, et al. Membrane cholesterol efflux drives tumor-associated macrophage reprogramming and tumor progression. Cell Metab. 2019;29:1376–1389.e4. https://doi.org/10.1016/j.cmet.2019.02.016.
19. Odegaard JI, Ricardo-Gonzalez RR, Goforth MH, Morel CR, Subramanian V, Mukundan L, et al. Macrophage-specific PPARgamma controls alternative activation and improves insulin resistance. Nature. 2007;447:1116–20. https://doi.org/10.1038/nature05894.

20. Missler M, Südhof TC. Neurexophilins form a conserved family of neuropeptide-like glycoproteins. J Neurosci. 1998;18:3630–8. https://doi.org/10.1523/JNEUROSCI.18-10-03630.1998.
21. Wang D, Zhang P, Liu Z, Xing Y, Xiao Y. NXPH4 promotes gemcitabine resistance in bladder cancer by enhancing reactive oxygen species and glycolysis activation through modulating NDUFA4L2. Cancers (Basel). 2022;14:3782. https://doi.org/10.3390/cancers14153782.
22. Yang Z, Wei B, Qiao A, Yang P, Chen W, Zhen D, et al. A novel EZH2/NXPH4/CDKN2A axis is involved in regulating the proliferation and migration of non-small cell lung cancer cells. Biosci Biotechnol Biochem. 2022;86:340–50. https://doi.org/10.1093/bbb/zbab217.
23. Qiao Q, Guo L, Ma Z. ETS1 facilitates the progression of OSCC and contributes to macrophage M2 polarization via regulating NXPH4. Cytotechnology. 2026;78:7. https://doi.org/10.1007/s10616-025-00869-6.
24. Sun X, Zhang Y, Zhang W, Jin L, Xin S. Targeting NXPH4/ALDH1L2 signaling suppresses enzalutamide resistance in prostate cancer. Cell Death Discov. 2026;12:91. https://doi.org/10.1038/s41420-026-02944-z.
25. Sun Z, Wang H, Xu Y, Liu Y, Wang L, Zhou R, et al. High expression of NXPH4 correlates with poor prognosis, metabolic reprogramming, and immune infiltration in colon adenocarcinoma. J Gastrointest Oncol. 2024;15:641–67. https://doi.org/10.21037/jgo-23-956.
26. Wei Y, Jiang Z, Song C, Qiao Y, Wang X, Ma W, et al. Fuzheng YiLiu decoction promote colorectal cancer apoptosis and reduce its proliferation via IGF2/IGF1R/PI3K/AKT pathway. Phytomedicine. 2025;148:157435. https://doi.org/10.1016/j.phymed.2025.157435.
27. Yang L-H, Lee RK-L, Kuo M-H, Miao C-C, Wang Y-X, Chen A, et al. Neuronal survival factor VGF promotes chemoresistance and predicts poor prognosis in lung cancers with neuroendocrine feature. Int J Cancer. 2022;151:1611–25. https://doi.org/10.1002/ijc.34193.
28. Jr Z, P H, Xj W, Zq W, Xc S-G, H W, et al. TNFRSF11B Suppresses Memory CD4 + T Cell Infiltration in the Colon Cancer Microenvironment: A Multiomics Integrative Analysis. Frontiers in immunology [Internet]. Front Immunol; 2021 [cited 2026 July 6];12. https://doi.org/10.3389/fimmu.2021.742358.
29. Alraouji NN, Colak D, Al-Mohanna FH, Alaiya AA, Aboussekhra A. Endogenous osteoprotegerin (OPG) represses ERα and promotes stemness and chemoresistance in breast cancer cells. Cell Death Discov. 2024;10:377. https://doi.org/10.1038/s41420-024-02151-8.
30. Siu L-S, Romanska H, Abel PD, Baus-Loncar M, Kayademir T, Stamp GWH, et al. TFF2 (trefoil family factor2) inhibits apoptosis in breast and colorectal cancer cell lines. Peptides. 2004;25:855–63. https://doi.org/10.1016/j.peptides.2003.11.023.
31. Dubeykovskaya ZA, Duddempudi PK, Deng H, Valenti G, Cuti KL, Nagar K, et al. Therapeutic potential of adenovirus-mediated TFF2-CTP-Flag peptide for treatment of colorectal cancer. Cancer Gene Ther. 2019;26:48–57. https://doi.org/10.1038/s41417-018-0036-z.
32. Sui L, Wang S, Ganguly D, El Rayes TP, Askeland C, Børretzen A, et al. PRSS2 remodels the tumor microenvironment via repression of Tsp1 to stimulate tumor growth and progression. Nat Commun. 2022;13:7959. https://doi.org/10.1038/s41467-022-35649-9.

33. Sun L, Gao X, Wang M, Zhang Y, Sun R, Chen Y, et al. Gobal crotonylome reveals that HNRNPC and its crotonylation promote p53-deficient tumor growth by stabilizing CCND1 and MCM3 mRNAs. Cancer Lett. 2025;628:217854. https://doi.org/10.1016/j.canlet.2025.217854.
34. Wang M, Pan Z, Chu X, Yao X, Duan X, Wan J, et al. Chemotherapy-induced PTEN-L secretion promotes the selection of PTEN-deficient tumor cells. J Exp Clin Cancer Res. 2024;43:140. https://doi.org/10.1186/s13046-024-03059-y.
35. Gebremeskel S, Johnston B. Concepts and mechanisms underlying chemotherapy induced immunogenic cell death: Impact on clinical studies and considerations for combined therapies. Oncotarget. 2015;6:41600–19. https://doi.org/10.18632/oncotarget.6113.
36. Cayrol C, Girard J-P. Interleukin-33 (IL-33): A nuclear cytokine from the IL-1 family. Immunol Rev. 2018;281:154–68. https://doi.org/10.1111/imr.12619.
37. Lotze MT, Tracey KJ. High-mobility group box 1 protein (HMGB1): Nuclear weapon in the immune arsenal. Nat Rev Immunol. 2005;5:331–42. https://doi.org/10.1038/nri1594.
38. Valenta T, Hausmann G, Basler K. The many faces and functions of β-catenin. EMBO J. 2012;31:2714–36. https://doi.org/10.1038/emboj.2012.150.
39. Zhu X, Lin S, Ruan L, Xiong J, Yao D, Wan H, et al. HNRNPC reprograms cancer metabolism to drive acquired chemoresistance in colorectal cancer by repressing of Nrf2/SLC7A11-dependent ferroptosis. Cell Commun Signal. 2025;24:26. https://doi.org/10.1186/s12964-025-02577-2.
40. Huang X-T, Chen J, Zhu E-L, Ma M-J, Yu Y-Y-H, Zhu Y-Q, et al. Positive feedback loop of histone lactylation-driven HNRNPC promotes autophagy to confer pancreatic ductal adenocarcinoma gemcitabine resistance. Adv Sci (Weinh). Weinheim, Baden-Wurttemberg, Germany; 2026;13:e10483. https://doi.org/10.1002/advs.202510483.
41. Wang Y, Yang T, Li Q, Zheng Z, Liao L, Cen J, et al. circASAP1 induces renal clear cell carcinoma ferroptosis by binding to HNRNPC and thereby regulating GPX4. Mol Cancer. 2025;24:1. https://doi.org/10.1186/s12943-024-02122-8.
42. Tian J, Zhang L, La X, Fan X, Li A, Wu C, et al. Tumor-secreted GRP78 induces M2 polarization of macrophages by promoting lipid catabolism. Cell Signal. 2023;108:110719. https://doi.org/10.1016/j.cellsig.2023.110719.
43. Daniel B, Nagy G, Horvath A, Czimmerer Z, Cuaranta-Monroy I, Poliska S, et al. The IL-4/STAT6/PPARγ signaling axis is driving the expansion of the RXR heterodimer cistrome, providing complex ligand responsiveness in macrophages. Nucleic Acids Res. 2018;46:4425–39. https://doi.org/10.1093/nar/gky157.
44. Chen J, Zhao D, Zhang L, Zhang J, Xiao Y, Wu Q, et al. Tumor-associated macrophage (TAM)-secreted CCL22 confers cisplatin resistance of esophageal squamous cell carcinoma (ESCC) cells via regulating the activity of diacylglycerol kinase α (DGKα)/NOX4 axis. Drug Resist Updat. 2024;73:101055. https://doi.org/10.1016/j.drup.2024.101055.
45. Zhang L, Lu X, Xu Y, La X, Tian J, Li A, et al. Tumor-associated macrophages confer colorectal cancer 5-fluorouracil resistance by promoting MRP1 membrane translocation via an intercellular

CXCL17/CXCL22-CCR4-ATF6-GRP78 axis. Cell Death Dis. 2023;14:582. https://doi.org/10.1038/s41419-023-06108-0.

46. Du Y, Chen Y, Yan Z, Yang J, Da M. Zinc finger protein 263 promotes colorectal cancer cell progression by activating STAT3 and enhancing chemoradiotherapy resistance. Sci Rep. 2024;14:21827. https://doi.org/10.1038/s41598-024-72636-0.
47. Cui J, Liu J, Fan L, Zhu Y, Zhou B, Wang Y, et al. A zinc finger family protein, ZNF263, promotes hepatocellular carcinoma resistance to apoptosis via activation of ER stress-dependent autophagy. Transl Oncol. 2020;13:100851. https://doi.org/10.1016/j.tranon.2020.100851.
48. Wang L, Li G, Zhou Z, Ge C, Chen Q, Liu Y, et al. Chromatin-associated OGT promotes the malignant progression of hepatocellular carcinoma by activating ZNF263. Oncogene. 2023;42:2329–46. https://doi.org/10.1038/s41388-023-02751-1.
49. Xu J, Zhou Y, Wang Q, Liu Y, Tang J. Zinc finger protein 263 upregulates interleukin 33 and suppresses autophagy to accelerate the malignant progression of non-small cell lung cancer. Clin Transl Oncol. 2024;26:924–35. https://doi.org/10.1007/s12094-023-03325-z.
50. Yu Z, Feng J, Wang W, Deng Z, Zhang Y, Xiao L, et al. The EGFR-ZNF263 signaling axis silences SIX3 in glioblastoma epigenetically. Oncogene. 2020;39:3163–78. https://doi.org/10.1038/s41388-020-1206-7.

Figures

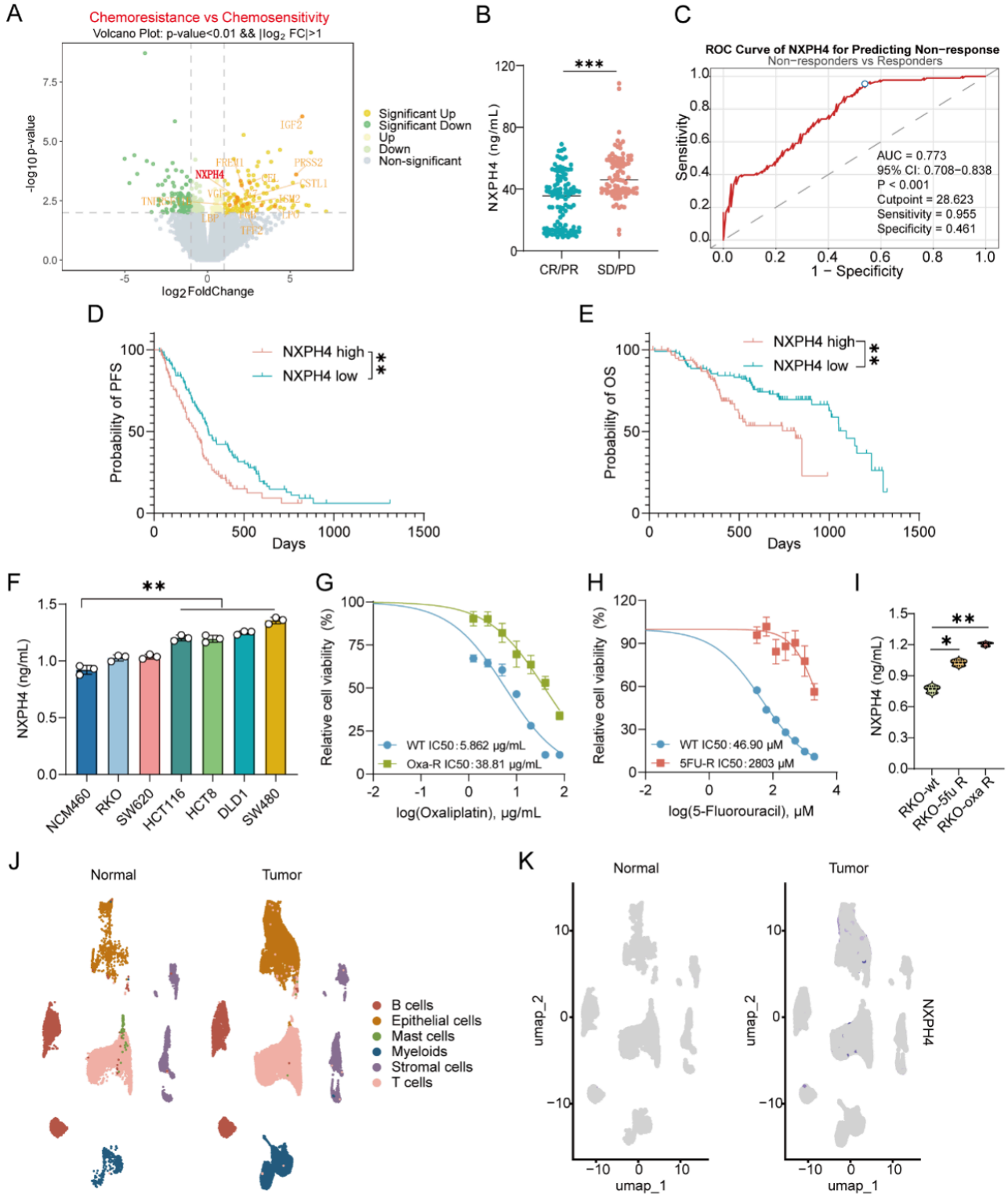


Figure 1

NXPH4 is upregulated in CRC and associated with chemoresistance and poor prognosis. (A) Volcano plot illustrating differential expression of nine secreted proteins in chemoresistant tissues, with NXPH4 showing significant upregulation. (B) Plasma NXPH4 levels in patients with distinct chemotherapy responses. (C) ROC curve of plasma NXPH4 for predicting chemotherapy efficacy. (D, E) Kaplan–Meier analysis of OS and PFS in patients stratified by median plasma NXPH4 concentration into high- (n = 95)

and low-expression (n = 95) groups. (F) ELISA measurement of NXPH4 secretion in the culture supernatants of normal intestinal epithelial cells and CRC cell lines. (G, H) CCK-8 assay determining the half-maximal inhibitory concentration (IC50) of oxaliplatin (Oxa) and 5-fluorouracil (5-FU) in RKO parental and drug-resistant cell lines. (I) ELISA quantification of NXPH4 levels in the culture supernatants of RKO parental and drug-resistant cells. (J, K) Single-cell transcriptome analysis of human colorectal cancer and normal tissues from the GSE132465 dataset. U-MAP visualization showing the annotated cell-type clusters segregated from normal and tumor tissues(J), U-MAP plots displaying the expression distribution of NXPH4 across distinct cell populations in normal and tumor samples(K). *$p < 0.05$, ** $p < 0.01$.

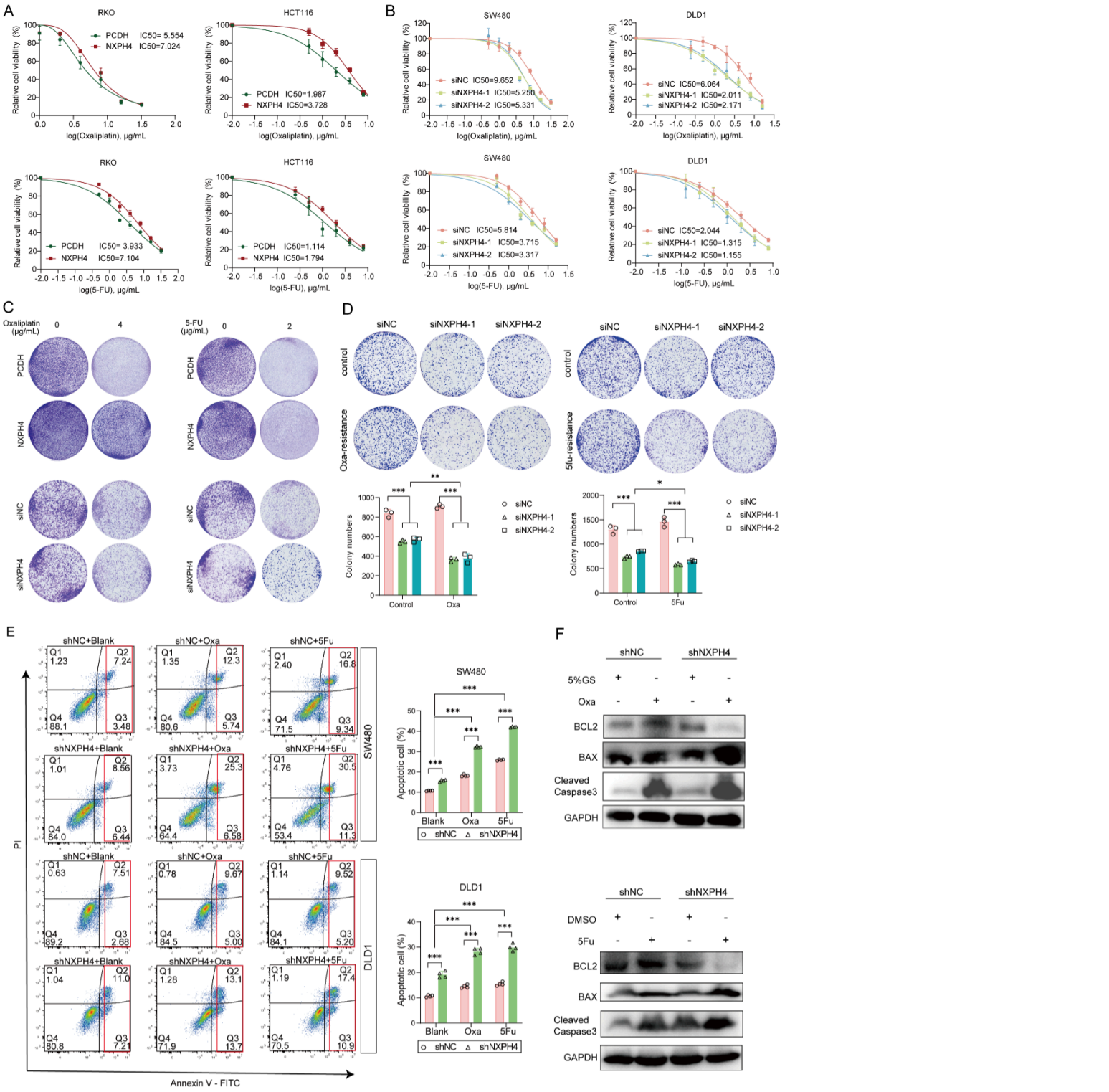


Figure 2

NXPH4 promotes CRC cell proliferation and chemoresistance in CRC cells. (A) CCK-8 assay determining IC50 of Oxa and 5-FU in NXPH4-overexpressing RKO and HCT116 cells (48 h). (B) CCK-8 assay determining IC50 curves of Oxa and 5-FU in NXPH4-knockdown SW480 and DLD1 cells (48 h). (C) Colony formation of CRC cells with NXPH4 overexpression or knockdown treated with Oxa and 5-FU. (D) Colony formation assay assessing cell proliferation in Oxa- and 5-FU-resistant cells upon stable NXPH4

knockdown. (E) Annexin V-FITC/PI double-staining flow cytometry detecting apoptosis rates in NXPH4-knockdown SW480 and DLD1 cells treated with Oxa and 5-FU for 48 h. (F) Western blot analysis of apoptosis-related proteins (BCL2, BAX, Caspase-3, and Cleaved caspase-3) in control and NXPH4-knockdown cells treated with Oxa and 5-FU for 48 h. * $p < 0.05$, ** $p < 0.01$, *** $p < 0.001$.

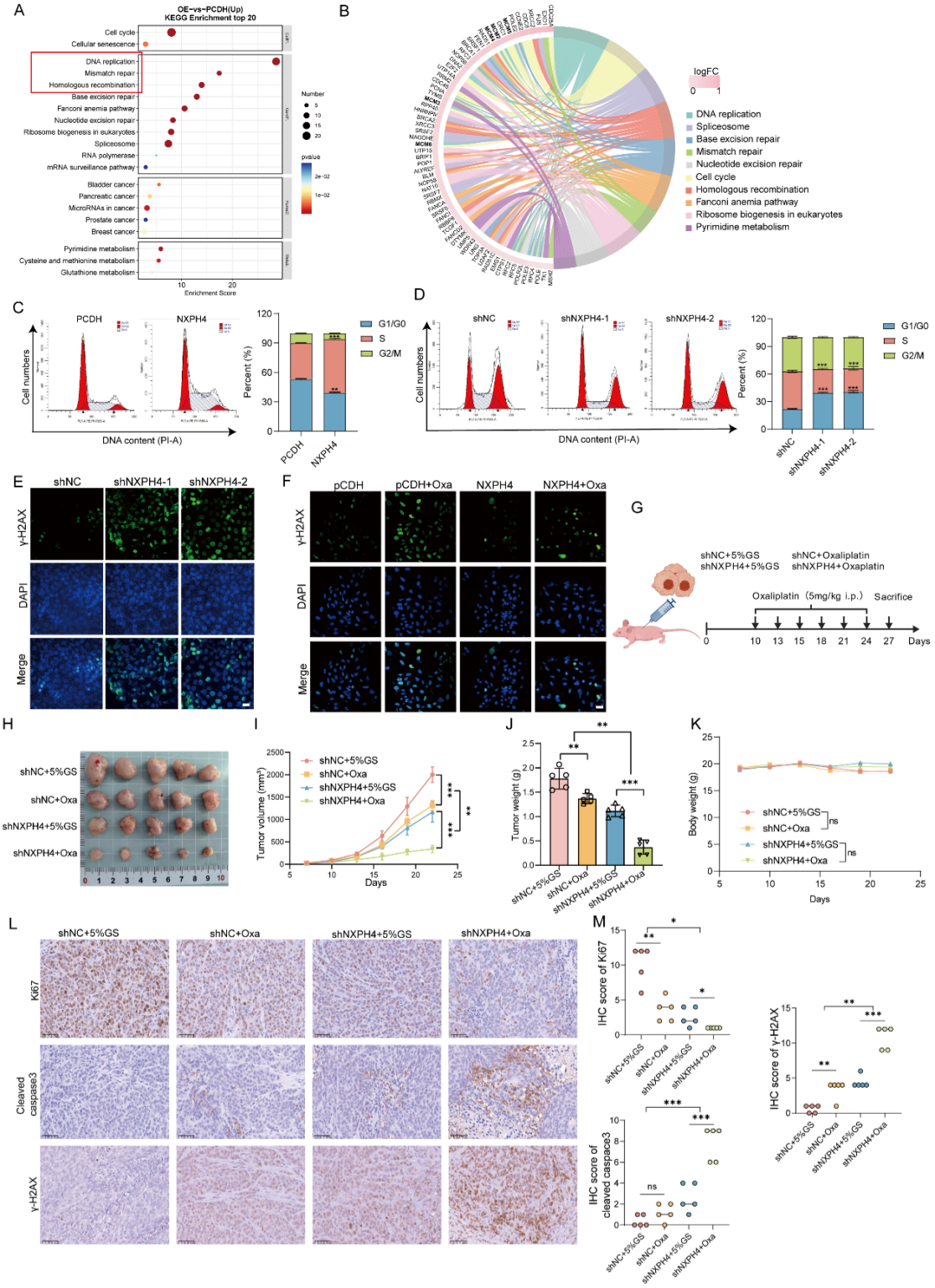


Figure 3

NXPH4 promotes chemoresistance through DNA damage repair mechanisms in vitro and in vivo. (A) Bulk RNA-seq of stable NXPH4-overexpressing RKO cells. KEGG pathway enrichment analysis showing significantly upregulated pathways compared with the control. (B) Chord diagram depicting the relationships between significantly upregulated pathways (DNA repair, cell cycle, etc.) and related DEGs in the NXPH4-overexpression group. (C) Flow cytometry analysis of cell cycle distribution in stable NXPH4-overexpressing RKO and HCT116 cells (PI staining). (D) Flow cytometry analysis of cell cycle distribution in stable NXPH4-knockdown SW480 cells. (E) Immunofluorescence staining of γ-H2AX in NXPH4-knockdown SW480 cells; scale bar, 20 μm. (F) Immunofluorescence staining of γ-H2AX in stable NXPH4-overexpressing RKO cells following Oxa treatment for 48 h; scale bar, 20 μm. (G) Schematic illustration of the animal experimental protocol. (H) Representative images of subcutaneous tumors in each group at the endpoint. (I) Tumor volume growth curves during treatment (measured every 3 days). (J) Tumor weight in each group at the endpoint. (K) Body weight changes of mice in each group during treatment. (L) IHC staining of Ki67, Cleaved caspase-3, and γ-H2AX in subcutaneous tumor tissues; scale bar, 50 μm. (M) Semi-quantitative IHC scores of Ki67, Cleaved caspase-3, and γ-H2AX in tumor tissues of each group. ns $p > 0.05$, * $p < 0.05$, ** $p < 0.01$, *** $p < 0.001$.

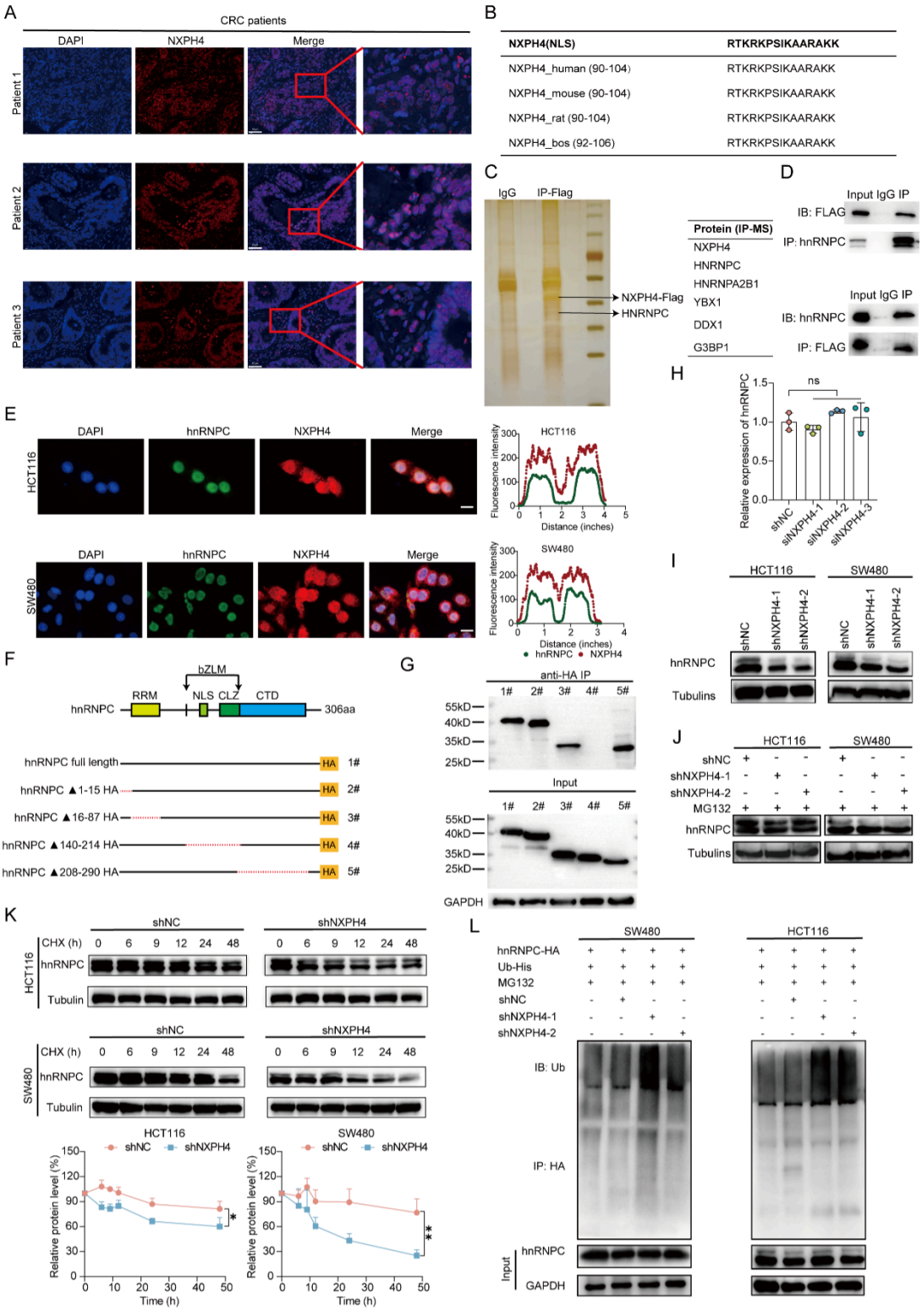


Figure 4

Nuclear-localized NXPH4 promotes DNA damage repair through the hnRNPC-MCM2-7 axis. (A) Immunofluorescence staining of colorectal cancer tissue showing the subcellular localization of NXPH4 (red); DAPI (blue); scale bar, 50 μm. (B) NLStradamus prediction of NXPH4 NLS in the 90–106 aa region (cross-species conservation). (C) Anti-Flag IP in Flag-NXPH4 RKO cells; silver staining and MS identification of NXPH4-interacting proteins. (D) Co-IP validation of exogenous NXPH4-hnRNPC

interaction in RKO cells. (E) Immunofluorescence showing colocalization of NXPH4 (red) and hnRNPC (green) in NXPH4-overexpressing RKO cells; DAPI (blue); scale bar, 20 μm. (F) Schematic of full-length hnRNPC (1–290 aa) and four HA-tagged truncated mutants (Δ1–15, Δ16–87, Δ140–214, Δ208–290). (G) Co-IP of NXPH4-Flag with full-length or truncated hnRNPC-HA in co-transfected HEK-293T cells (48 h). (H) SW480 cells were transfected with siNXPH4, and hnRNPC mRNA levels were quantified by RT-qPCR. (I) Western blot of hnRNPC in NXPH4-knockdown HCT116 and SW480 cells. (J) Western blot of hnRNPC in NXPH4-knockdown HCT116 and SW480 cells treated with MG-132 (10 μM, 6 h). (K) Western blot of hnRNPC half-life (up) and quantification (down) in NXPH4-knockdown and shNC cells treated with CHX (50 μg/mL) for the indicated times. (L) Anti-HA IP and Western blot of hnRNPC ubiquitination in NXPH4-knockdown and shNC cells co-transfected with hnRNPC-HA and Ubiquitin, treated with MG-132 (10 μM, 6 h). * $p < 0.05$, ** $p < 0.01$, *** $p < 0.001$.

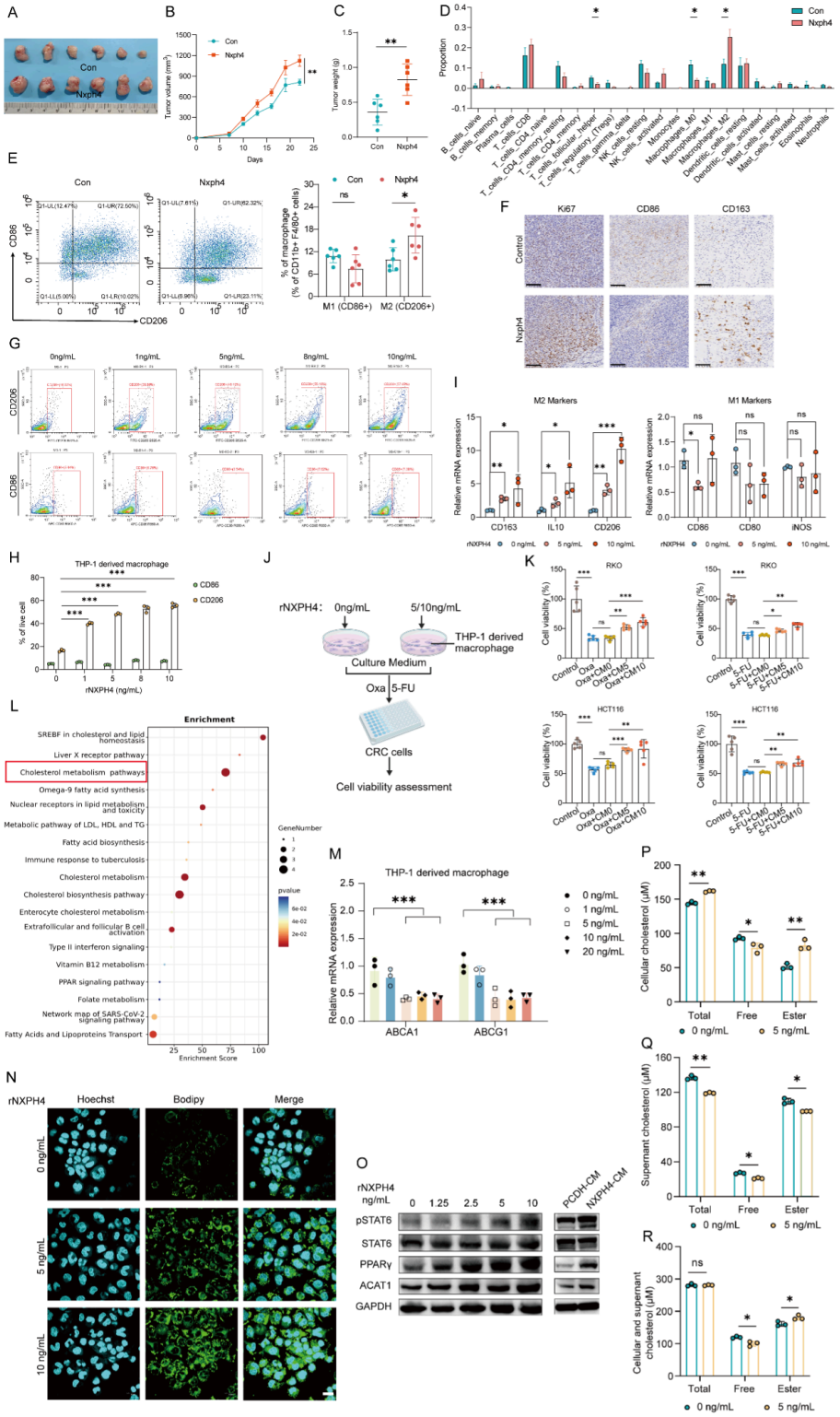


Figure 5

NXPH4 induces M2 macrophage polarization through cholesterol metabolism reprogramming. (A-C) Subcutaneous MC38 xenografts in C57BL/6 mice (n = 6/group) overexpressing murine Nxph4 or control. Tumor growth curves (B) and endpoint weights (C) were monitored every 3 days until day 22. (D) CIBERSORTx analysis of tumor-infiltrating immune cell proportions from Bulk RNA-seq of Nxph4-overexpressing MC38 tumors. (E) Flow cytometry of M1 (F4/80+CD11b+CD86+) and M2

(F4/80+CD11b+CD206+) macrophages in MC38 tumors. (F) IHC staining of Ki67, CD86 and CD163 in MC38 tumors; scale bar, 50 μm. (G, H) THP-1-derived M0 macrophages (PMA 200 ng/mL, 24 h) treated with rNXPH4 (0, 5, 10 ng/mL) for 48 h. Flow cytometry of CD86+ and CD206+ populations (G) and quantification (H). (I) RT-qPCR of M2 (CD163, IL-10, CD206) and M1 (CD86, CD80, iNOS) markers in M0 macrophages treated with rNXPH4 (0, 5, 10 ng/mL) for 48 h. (J) Schematic workflow: conditioned medium from rNXPH4-treated M0 macrophages (0, 5, 10 ng/mL, 48 h) combined with Oxa or 5-FU for CRC cell treatment. (K) CCK-8 assay of RKO cell viability after 48 h treatment with macrophage-conditioned medium plus Oxa or 5-FU. (L) KEGG enrichment of altered metabolic pathways from Bulk RNA-seq (n = 3) of THP-1 M0 macrophages treated with 5 ng/mL rNXPH4 for 48 h. (M) RT-qPCR of cholesterol efflux genes ABCA1 and ABCG1 in THP-1 M0 macrophages treated with rNXPH4 (0, 5, 10 ng/mL) for 48 h. (N) BODIPY 493/503 (Beyotime, C2053S) staining of lipid droplets in rNXPH4-treated macrophages; Hoechst 33342 (blue); scale bar, 20 μm. (O) Western blot of p-STAT6, STAT6, PPARγ, and ACAT1 in rNXPH4-treated macrophages. (P) Amplex Red assay (Beyotime, S0221S) of total, free, and esterified cholesterol in macrophage lysates. (Q) Cholesterol content in corresponding culture supernatants. (R) Combined analysis of total cholesterol in cells and supernatants.* $p < 0.05$, ** $p < 0.01$, *** $p < 0.001$.

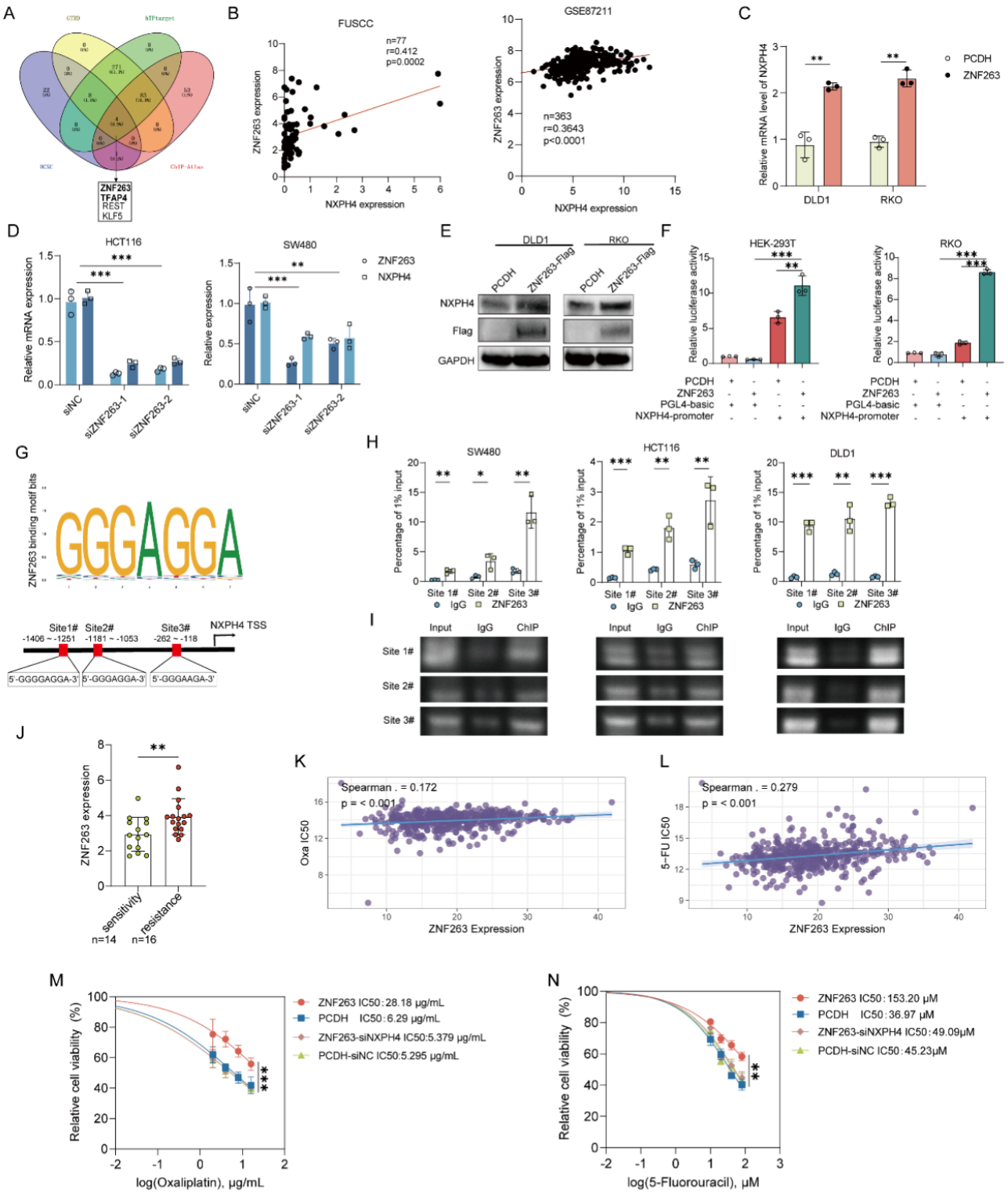


Figure 6

ZNF263 activates NXPH4 transcription to promote chemoresistance. (A) Integration of UCSC, ChIP-Atlas, GTRD, and hTFtarget databases predicting TFs regulating NXPH4 expression; intersection screening identified four candidate TFs. (B) Spearman correlation of ZNF263 and NXPH4 expression in FUSCC CRC transcriptome data (n = 77) and GSE87211 dataset (n = 363). (C) Lentiviral-mediated stable ZNF263 overexpression in DLD1 and RKO cells; RT-qPCR of NXPH4 mRNA. (D) Transient ZNF263

knockdown in HCT116 and SW480 cells; RT-qPCR of NXPH4 mRNA. (E) Western blot of NXPH4 in stable ZNF263-overexpressing DLD1 and RKO cells. (F) NXPH4 promoter (-2000 to + 100 bp) cloned into pGL4.10 and co-transfected with TK reference plasmid (50:1) into ZNF263-overexpressing RKO cells; dual-luciferase reporter assay at 24 h. (G) JASPAR prediction of ZNF263 DNA-binding motif (top) and schematic of three predicted ZNF263 binding sites (Site 1–3) within the NXPH4 promoter (-2000 to + 100 bp) (bottom). (H, I) Flag ChIP in ZNF263-Flag-overexpressing SW480, DLD1, and HCT116 cells; ChIP-qPCR validation of ZNF263 enrichment at the three predicted NXPH4 promoter binding sites. (J) ZNF263 expression in chemoresistant (n = 16) versus chemosensitive (n = 14) CRC tissues from FUSCC clinical samples. (K, L) Spearman correlation of ZNF263 expression with predicted Oxa (K) and 5-FU (L) IC50 in TCGA CRC patients using the oncoPredict package (GDSC and CTRP databases). (M, N) CCK-8 assay of Oxa (M) and 5-FU (N) IC50 in stable ZNF263-overexpressing RKO and HCT116 cells transiently transfected with siNXPH4 (48 h). * $p < 0.05$, ** $p < 0.01$, *** $p < 0.001$.

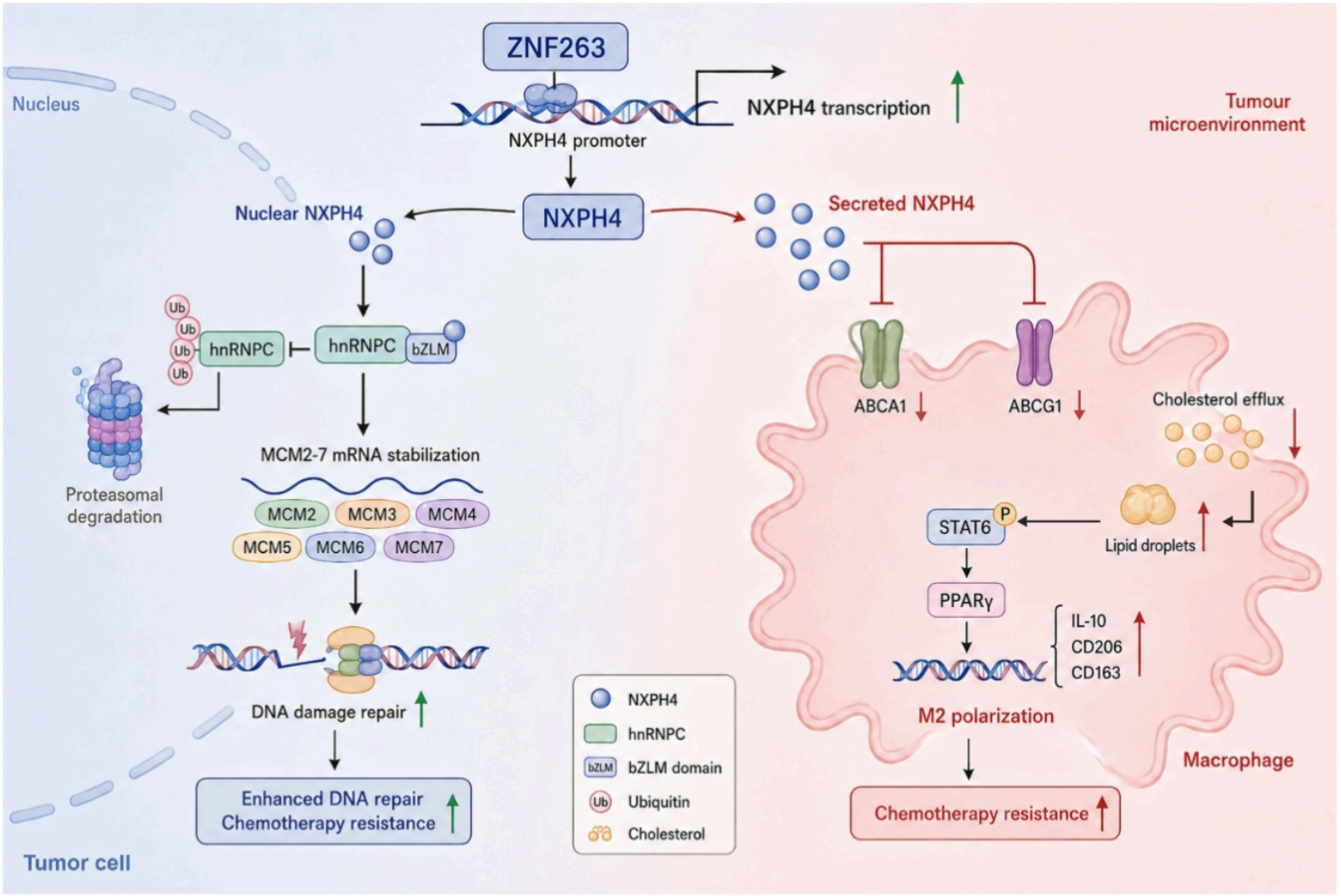


Figure 7

NXPH4, a transcriptional target of ZNF263, promotes chemoresistance in colorectal cancer by enhancing DNA damage repair and inducing M2 macrophage polarization. The transcription factor ZNF263 directly binds to the NXPH4 promoter to activate its transcription. Nuclear NXPH4 interacts with the bZLM domain of hnRNPC, inhibiting hnRNPC ubiquitin-proteasome degradation, stabilizing MCM2-7

mRNA, and promoting DNA damage repair. Secreted NXPH4 downregulates ABCA1/ABCG1 expression in macrophages, suppresses cholesterol efflux, promotes lipid droplet accumulation, and activates the STAT6-PPARγ signaling axis to drive M2 polarization, thereby further promoting chemoresistance.

Supplementary Files

This is a list of supplementary files associated with this preprint. Click to download.

- SupplementalFigureS1S3.docx
- SupplementalTableS1S4.docx
- supplementaryfilegelsandblots.pdf